ACS APPLIED ENERGY MATERIALS

Letter

Cite This: ACS Appl. Energy Mater. 2020, 3, 176−183

www.acsaem.org

Hydrogen Evolution by Ni_2P Catalysts Derived from Phosphine MOFs

Oluwaniyi Mabayoje,[†] Samuel G. Dunning,[†] Kenta Kawashima,[†] Bryan R. Wygant,[†] Ryan A. Ciufo,[†] Simon M. Humphrey,*[,†,§] and C. Buddie Mullins*[,†,‡,§]

[†]Department of Chemistry, University of Texas at Austin, Austin, Texas 78712, United States

[‡]Department of Chemical Engineering, University of Texas at Austin, Austin, Texas 78712, United States

[§]Texas Materials Institute, University of Texas at Austin, Austin, Texas 78712, United States

Supporting Information

ABSTRACT: Strategies to improve the catalytic efficiency of the hydrogen evolution reaction (HER), an integral electrochemical reaction in solar-to-hydrogen technologies, frequently include the use of porous precursors to make electrocatalysts. Researchers have used high-surface-area metal organic frameworks (MOFs) as precursors to synthesize active metal phosphide catalysts, but these MOFs must be mixed with a second phosphorus precursor to produce the metal phosphide. In this work, we synthesized nickel phosphide catalysts in one step from single-MOF precursors. Our MOFs contain phosphine coordination sites within the organic framework, allowing us to produce metal phosphide catalysts without the need for an exogenous phosphorus source. This strategy is convenient because the use of a crystalline precursor may offer the possibility of greater control over both the phase and resulting properties of the as-formed metal phosphide materials. The best MOF-derived Ni_2P HER electrocatalyst delivered current densities of −10 mA/cm^2 at an overpotential of 120 mV on glassy carbon substrate electrodes. A long-term test showed our sample could evolve hydrogen for over 1 h under physically and chemically harsh conditions.

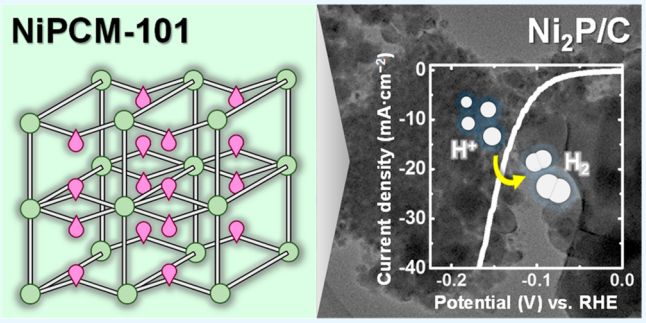

KEYWORDS: *electrocatalyst, energy conversion, hydrogen evolution, metal organic framework, phosphine coordination material, nickel phosphide*

1. INTRODUCTION

The development of electrocatalysts for the hydrogen evolution reaction (HER) is of great importance in photoelectrochemical water splitting and photovoltaic electrolysis, processes that can provide hydrogen as a carbon-neutral source of energy.[1,2] Hydrogen produced from water using solar energy can be collected and used in devices like fuel cells, or as a chemical feedstock, thus achieving the goal of converting an intermittent source of energy like the sun into chemical fuel that can be stored.[3−5] The best catalysts for the HER are typically costly noble metals (e.g., platinum, palladium); this has promoted increased research efforts aimed at discovering efficient replacement catalysts based on more earth-abundant and inexpensive transition metals, such as the iron group metals.[6−9] Progress has been made in the past decade, with non-noble metal catalysts showing high activity in the form of low "overpotentials" (defined here as the additional potential needed to achieve a current density of −10 mA/cm^2).[10−12]

A tremendous amount of work has recently been dedicated to metal phosphide catalysts.[13−17] These materials show the lowest overpotentials recorded in the literature, and examples include electrocatalysts such as iron,[18,19] cobalt,[15,16,20] nickel,[13,14] tungsten,[21,22] and molybdenum phosphide phases.[23] Metal phosphides are generally made by the colloidal conversion of metal nanoparticles to their phosphides using phosphorus precursors such as trioctylphosphine[13,16] or by phosphidization of nanostructured templates of metals and metal oxides in a furnace with phosphorus precursors like sodium hypophosphite (NaH_2PO_2) or phosphorus.[14,15] These types of phosphorus precursors are toxic, explosive, and/or pyrophoric and therefore present inherent handling problems for scale-up. Therefore, P(III)-based organophosphorus compounds such as trialkyl and triarylphosphines are attractive alternatives, providing they can be successfully incorporated into the metal phosphide precursor mixtures. These electrocatalysts are typically nanostructured materials with high surface areas, and examples include nanorods,[24] nanowires,[18] and hollow nanoparticles.[13,25] Surface area directly influences the geometric activity of catalysts, and new methods to synthesize porous or high-surface-area versions of these metal

Received: October 28, 2019
Accepted: December 9, 2019
Published: December 9, 2019

DOI: 10.1021/acsaem.9b02109
ACS Appl. Energy Mater. 2020, 3, 176−183

Scheme 1. (I) Cnventional Synthesis of a Metal Phosphide by Combining Phosphorus and MOF Precursors and (II) the Novel Synthesis of a Metal Phosphide from a Single-Source Crystalline MOF Precursor

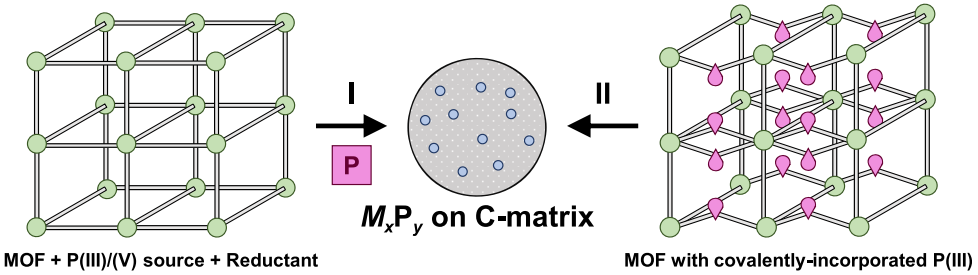

phosphide materials are of great interest to researchers, as these materials are valuable in many catalytic reactions including water splitting electrocatalysis,[26] and hydroprocessing (hydrodesulfurization and hydrodeoxygenation) catalysis.[27,28]

Strategies to increase the surface area of catalysts in water splitting include making small nanoparticles (sub 20 nm)[13,16] and depositing materials on high-surface-area supports such as carbon fiber paper or carbon nanotubes.[29,30] For example, Sun and co-workers found that the overpotential required for CoP to drive a current density of −10 mA/cm^2 was reduced from 226 to 122 mV when the catalyst was prepared on a carbon nanotube support.[29] Another common approach to attain high-surface-area catalysts is to make metal phosphides from porous precursors. Thus, research on converting high-surface-area metal organic frameworks (MOFs) into metal phosphides has recently gained interest in electrocatalysis. MOF-derived catalysts are usually prepared by heating MOFs in a furnace along with NaH_2PO_2 or phosphorus at temperatures ranging from 300 to 750 °C.[31−34] An advantage of this strategy is that the metal phosphide catalyst usually retains some of the high surface area and porous structure of the initial MOF. Additionally, these MOF-derived materials sometimes retain the morphology of the initial MOF, leading to unique nanostructures for metal phosphide catalysts.[32] Finally, the organic ligands in the MOFs are frequently converted into a porous carbon matrix, with the metal phosphide nanoparticles homogeneously distributed within the conductive carbon material, improving charge transfer.[32] The carbon layer also serves to protect the catalyst from the highly corrosive reaction conditions in electrocatalysis, improving the lifetime of the catalyst.[35]

Phosphine coordination materials (PCMs) are a unique class of MOF materials synthesized from functionalized aryl-phosphine building blocks. These frameworks contain a high density of Lewis-basic phosphine sites which can be *post*-synthetically modified to incorporate secondary metals[36,37] or *pre*-synthetically modified to incorporate phosphine oxide[38−40] or alkyl phosphonium[41,42] species. It is our belief that these phosphorus-rich PCMs are ideally suited as single-source metal phosphide precursors, in which the *M*:P ratio can be finely controlled on the basis of the well-defined composition of the crystalline precursors. Further, PCMs are air-stable precursors that can be prepared at scale and contain abundant, labile P(III) sites as the P source. As the structures of these PCMs are highly modifiable and can be resolved by single-crystal X-ray diffraction (XRD), this strategy could more broadly offer a convenient and repeatable method to control the stoichiometry, phase-purity, and other properties of the derived metal phosphides. Herein we report the first examples of this premise, in which we demonstrate the synthesis and characterization of several nickel phosphide HER catalysts in one step, using PCMs as single-source metal phosphide precursors (Scheme 1). To the best of our knowledge, this is the first example of nickel phosphide HER catalysts formed by this convenient route. We have characterized the catalytic properties of these materials, as well as their morphology and crystallinity, and found that the different phases of nickel phosphides (i.e., Ni_2P and $Ni_{12}P_5$) formed depend on the annealing temperature of the Ni-MOFs. Importantly, we discovered that these catalysts, on nonporous inert substrates [e.g., a glassy carbon (GC) electrode], were highly active for the HER, achieving current densities of −10 mA/cm^2 at a low overpotential of 120 mV.

Catalysts made up of nickel phosphide particles embedded in a carbon matrix were synthesized from a single-MOF precursor, Ni(II)PCM-101.[37] This material is a 3D microporous MOF based on triarylphosphine (Ar_3P) building blocks and was obtained by slowly heating solutions of $Ni(BF_4)_2$ with tris(p-carboxylato)triphenylphosphine ($P\{C_6H_4\text{-}4\text{-}CO_2H\}_3$; $tctpH_3$) and 4,4′-bipyridine (bipy) ligands. PCM-101 has the formula $[Ni_6(\mu_3\text{-}OH)_2(tctp)_4(4,4'\text{-}bipy)_3(HBF_4)]\cdot$solvate, with a corresponding Ni:P ratio of 6:4, making it an ideal candidate for the synthesis of nickel phosphides. The structure of PCM-101 can briefly be described as two-dimensional bilayer sheets of $tctp^{3-}$ and $[Ni_3(\mu_3\text{-}OH)]^{5+}$ nodes fused together into a three-dimensional array by interlayer bipy pillars. A more detailed description of its structure and properties can be found in the original publication.[37] The structural data for PCM-101 is also available free of charge from https://ccdc.cam.ac.uk/ in CIF format by clicking on "Access Structures" and using reference CCDC-1581200 with DOI: 10.1002/anie.201802402. Samples of NiPCM-101 were annealed at 350, 450, and 550 °C in a hydrogen atmosphere to form the nickel phosphide catalysts.

2. EXPERIMENTAL SECTION

2.1. Ni(II)PCM-101 Synthesis. NiPCM-101 [chemical formula: $(C_{114}H_{74}Ni_6N_6O_{26}P_4^{2-})_n$, HBF_4, $2(H_3O^+)$, $7(H_2O)$, $5(C_3H_7NO)$] was synthesized according to the literature procedure.[37]

2.2. Nickel Phosphide Synthesis. NiPCM-101 (∼25−50 mg) was transferred into an alumina crucible and then placed in an evacuated quartz tube. Hydrogen gas was flown into the tube at a flow rate of 50 sccm, and samples were annealed at specified temperatures (350, 450, and 550 °C) for 4 h. Then, the samples were cooled down to room temperature. The theoretical yield of Ni_2P (without a carbon shell) is ∼15 wt %.

2.3. Characterization. A Quanta FEG scanning electron microscopy (SEM) equipped with a Bruker Xflash 5010 detector and a JEOL, JEM-2010F high-resolution transmission electron microscope (HRTEM) were used for microscopy imaging. Powder

DOI: 10.1021/acsaem.9b02109
ACS Appl. Energy Mater. 2020, 3, 176−183

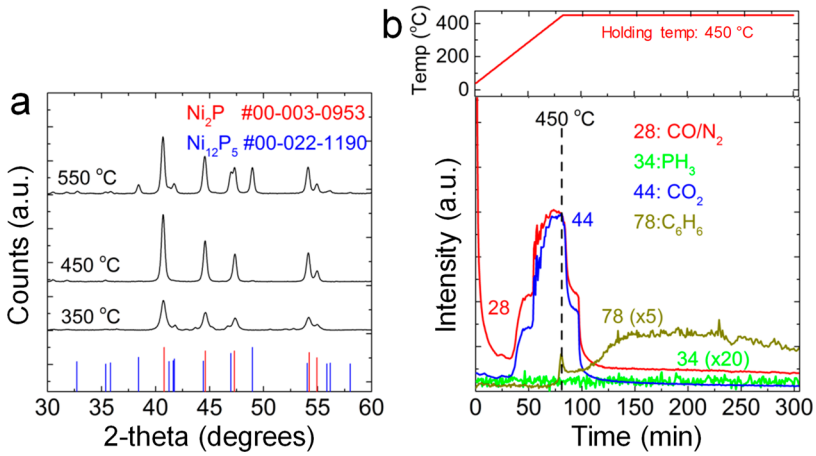

Figure 1. (a) PXRD patterns for NiPCM-101 samples annealed at 350, 450, and 550 °C. (b) QMS plots showing gaseous species formed when NiPCM-101 samples are annealed in a H_2 atmosphere.

XRD (PXRD) patterns were acquired with a Spider (Rigaku) diffractometer with a Cu Kα radiation source. A Kratos Axis Ultra Spectrometer with a monochromated Al Kα source was used to take X-ray photoelectron spectroscopy (XPS) data of annealed NiPCM-101 samples. A quadrupole mass spectrometry (QMS) system was used for residual gas analysis (RGA) studies on the effluent stream during annealing. Approximately 250 mg of the sample was supported on a quartz wool plug in a quartz tube and held in an Applied Test Systems model 3210 tube furnace. MKS type M100B mass flow controllers were used to deliver H_2 to the sample bed. The effluent was monitored using a custom-built gas analysis system consisting of an Extorr XT100 residual gas analyzer operating in a stainless-steel chamber with a base operating pressure of 5.0×10^{-10} Torr. Effluent gas was introduced to the analysis chamber at a pressure of 9.0×10^{-7} Torr through a temperature-controlled leak valve.

2.4. Electrochemical Tests. All potentials were recorded against a Ag/AgCl (saturated KCl) reference electrode with Teflon frits from CH Instruments and reported against the reversible hydrogen electrode (RHE), except where otherwise noted. Working electrodes were prepared by sonicating 2 mg of our samples in 0.4 mL of isopropanol. This mixture was sonicated for 30 min to form a homogeneous suspension that was then drop-cast on a ~0.19625 cm^2 GC electrode (mass loading: 0.5 mg/cm^2). We estimated the HER activity of electrodes using cyclic voltammetry (CV). First, we carried out 25 CV scans (no *iR* drop correction) from −0.2 to −0.4 V vs Ag/AgCl at a scan rate of 100 mV/s, and then a linear sweep voltammetry scan at a scan rate of 10 mV/s from −0.2 to −0.4 V vs Ag/AgCl was recorded for all samples. An amperometric stability test was performed on our best-performing NiPCM-101-450 sample at −0.138 V vs RHE over 1 h. To check the stability, 0.01 mL of 0.1 wt % Nafion solution was introduced to enhance the physical stability of the resultant catalyst film, and the rotation disk electrode system was used at the rotation speed of 1600 rpm. Unless otherwise noted, the *iR* drop was corrected for all the electrochemical tests. Additionally, all the electrochemical tests were conducted in a degassed 0.5 M H_2SO_4 electrolyte (pH ~ 0.3).

3. RESULTS AND DISCUSSION

3.1. Characterization of Nickel Phosphides. To begin our analysis, we studied the transformation of NiPCM-101 samples to nickel phosphides in a hydrogen atmosphere at varying temperatures using PXRD measurements (Figure 1a). When the MOF precursor is annealed at 350 °C in hydrogen, diffraction peaks in the PXRD pattern are indexed to hexagonal Ni_2P (JCPDS 00-003-0953) along with additional relatively weak peaks belonging to a $Ni_{12}P_5$ phase (JCPDS 00-022-1190). Increasing the annealing temperature to 450 °C yielded a similar diffraction pattern with peaks indexable to the Ni_2P phase. PXRD plots for samples annealed at 550 °C also show peaks belonging to Ni_2P, along with a reappearance of the $Ni_{12}P_5$ phase. This indicates that the pure Ni_2P phase forms in a narrow temperature range around 450 °C.

Thermogravimetric analysis (TGA) of NiPCM-101 shows that these materials are stable up to 340 °C.[37] Above this temperature, however, the MOF begins to undergo thermal degradation, initiated by decomposition of the organic components. The first step in this process is decarboxylation to yield CO_2 gas; at increasingly higher temperatures, the remaining organic components are degraded with the evolution of other volatile gases, accompanied by the formation of the desired nickel phosphide catalyst. We used a QMS to analyze the gaseous species produced during the synthesis of Ni_2P from NiPCM-101 in order to gain more information about the solid-state phosphidization process. Results presented in Figure 1b show that major products observed include NH_3 (m/z 17), H_2O (m/z 18), CO and N_2 (m/z 28), and CO_2 (m/z 44), all reasonable gas phase products that originate from the decomposition of the organic ligands surrounding nickel in the organic framework. We also detect C_6H_6 (m/z 78), a known product from the decomposition of triphenylphosphine. Importantly, we did not detect any mass 34 species representing phosphine (PH_3) in our QMS studies. It has been suggested that phosphine gas that evolved from phosphorus sources like NaH_2PO_2 is involved in the transformation of precursors to metal phosphide.[43] Instead, our results indicate that, for our system, the formation of the metal phosphide proceeds as a clean, direct solid-state reaction between the Ni and P components within the PCM at high temperature.

At elevated temperatures, the MOF could also undergo sintering, leading to a reduced bulk surface area. To probe this, we used a double layer capacitance (C_{dl}) method (Figure S1) to determine the electrochemically active surface area (ECSA) of the samples annealed at 450 °C. The experiment showed that the catalyst possesses an ECSA of 76 m^2/g, double that of the surface area for 21 nm Ni_2P samples (32.8 ± 0.2 m^2/g),[13] and also higher than the 48 m^2/g surface area observed for ~9 nm Ni_2P nanocrystals.[44] This surface area also compares well to Ni_2P nanosheets prepared by conversion of Ni nanosheets (68 m^2/g).[45] Our results indicate that, while the final catalysts exhibit some sintering upon annealing, the Ni_2P materials

DOI: 10.1021/acsaem.9b02109
ACS Appl. Energy Mater. 2020, 3, 176−183

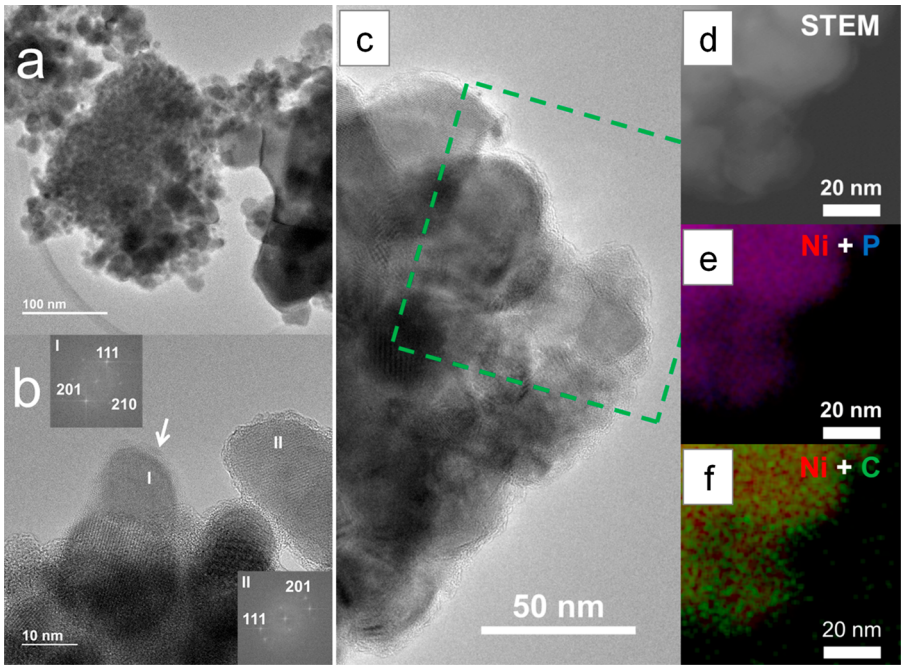

Figure 2. (a) Low-resolution TEM image of 450 °C Ni_2P sample showing the dispersity of particle sizes. (b) HRTEM image of the same sample, with FFT insets confirming the Ni_2P phase of two particles near the surface (I and II). An amorphous carbon coating is clearly visible surrounding each particle (white arrow). (c) TEM image of 450 °C sample; the green box denotes the EDX analysis area. (d) Scanning TEM image of Ni_2P sample with EDX maps of (e) Ni + P (*red* and *blue*, respectively) and (f) Ni + C (*red* and *green*, respectively).

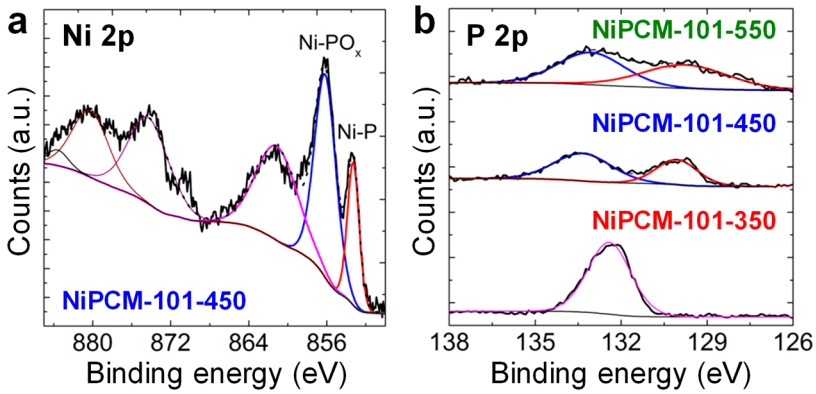

Figure 3. (a) XPS Ni 2p region for NiPCM-101 samples annealed at 450 °C for 4 h showing the presence of oxidized nickel species on the surface of Ni_2P samples. (b) The XPS P 2p region for NiPCM-101 samples annealed at 350, 450, and 550 °C.

prepared in our experiments benefit from the high surface area of the parent MOF precursor (ca. 315 m^2/g).

To better understand how the catalysts' structure and morphology relate to the measured surface area, we performed SEM (Figure S2) and HRTEM (Figure 2) analysis of the annealed catalysts. SEM images show that the samples, regardless of annealing temperatures, are made up of sub-100 nm particles agglomerated into micron-sized aggregates. We used energy-dispersive X-ray spectroscopy (EDX; Figure S3) measurements to perform bulk compositional analysis of the nickel phosphides obtained by annealing NiPCM-101 in H_2. Samples annealed at 350 and 450 °C show a Ni:P ratio of ∼2:1 while the sample annealed at 550 °C showed a slightly higher Ni content, consistent with the observation of a slightly nickel-rich $Ni_{12}P_5$ phase seen in X-ray diffractograms. A closer inspection of the samples under TEM shows that samples obtained after annealing NiPCM-101 MOF precursors at 350 °C are polydisperse (Figure S4) with nanoparticle sizes ranging from 5 to 100 nm with most of the particles in the 5−40 nm range (average ca. 12.3 nm) in a carbon matrix with a ∼ 2 nm carbon shell surrounding these particles (Figure S5). TEM images of samples prepared at the slightly higher temperatures of 450 (Figure 2a) and 550 °C (Figure S6) reveal that the particles grow slightly larger (average ca. 17 and 24 nm, respectively) and the carbon shell surrounding these particles is thinner (<2 nm) than those surrounding samples prepared at 350 °C. From these images, the high surface area we observe is likely due to a combination of the nanoscale dimensions of the nickel phosphide crystallites, as well as the amorphous carbon shell, which would be expected to have a high surface area.

We also investigated the crystalline phases of samples using selected area electron diffraction (SAED); a representative pattern of samples annealed at 450 is shown in Figure S7. Radial distribution plots generated from the SAED patterns for 450 °C annealed NiPCM-101 samples can be indexed to Ni_2P in agreement with PXRD measurements. The $Ni_{12}P_5$ phase is

DOI: 10.1021/acsaem.9b02109
ACS Appl. Energy Mater. 2020, 3, 176−183

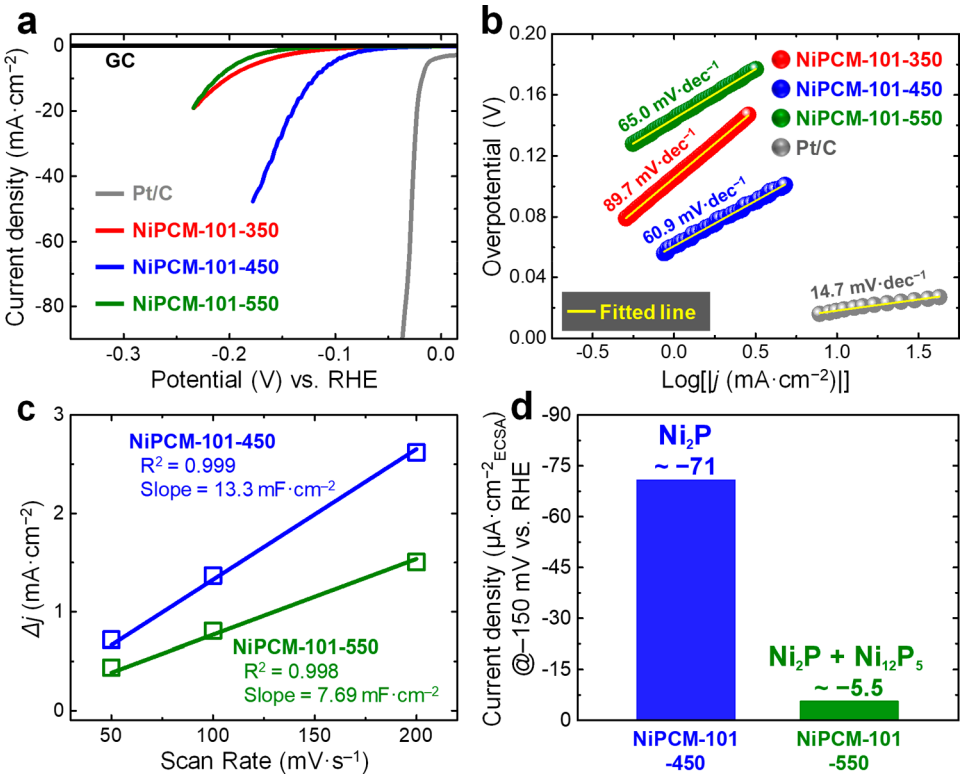

Figure 4. (a) LSV polarization curves for an annealed NiPCM-101 sample, benchmark Pt (Pt/C), and GC electrodes. (b) Corresponding Tafel plots for an annealed NiPCM-101 sample, Pt/C, and GC electrodes. (c) Charging current density differences (Δj at −0.05 V vs Ag/AgCl) plotted against different scan rates (50, 100, and 200 mV/s) for NiPCM-101-450 and -550 to determine the ECSAs. (d) Comparison of current densities based on ECSA for NiPCM-101-450 and -550.

also present in samples annealed at 350 and 550 °C (Figures S5 and S6). Fast Fourier transform (FFT) analysis of single particles in the samples also confirms the presence of these phases, as can be seen in Figure 2b. The FFT patterns can be indexed to the ⟨111⟩, ⟨201⟩, and ⟨210⟩ planes of Ni_2P, but there does not appear to be any preferential faceting in the particles. EDX elemental maps on the 350 °C (Figure S8) and 450 °C (Figure 2c−f) samples indicate that nickel and phosphorus are uniformly distributed in the core of nanoparticles, and an amorphous carbon layer can be clearly observed in these images.

XPS analysis was then used to gain vital insight into the elemental surface-concentrations and chemical states of the MOF-derived Ni_2P samples. Representative XPS spectra for annealed MOF samples are presented in Figure 3 and Figure S9. Deconvolution of the spectrum for high-resolution measurements in the Ni 2p region for the sample annealed at the intermediate temperature (450 °C) is presented in Figure 3a, and we detect peaks assigned to $Ni^{\delta+}$ (where $0 < \delta < 2$) at 853 eV in Ni_2P and Ni^{2+} in oxidized nickel phosphate-like species at 856 eV.[31,46] Since the photoelectrons ejected in these measurements only originate from the surface (<10 nm) of the samples being studied,[47] the chemical species observed may be partially oxidized and are likely different from those in the bulk of the micron-sized metal phosphide aggregates in our samples. Nevertheless, these measurements help in determining important information such as surface elemental compositions.

In general, we find that bulk elemental composition determined by EDX measurements and ratios expected from the major PXRD phases identified in our diffractograms are in agreement with elemental concentrations determined by XPS for samples annealed at 450 and 550 °C, with both samples showing a roughly 2:1 ratio of Ni:P. Samples annealed at 350 °C showed a surprisingly high phosphorus content, with a P:Ni ratio of 8, suggesting phosphorus enrichment on the surface of samples annealed at lower temperatures. Deconvolution of the measurements taken in the P 2p region (Figure 3b) for the sample annealed at 350 °C shows that the phosphorus present on the surface of this sample is in the form of organic phosphate species, likely indicating the MOF is not fully decomposed at low temperatures. This is distinct from the phosphorus species observed in samples annealed at higher temperatures, which show only phosphidic (Ni−P) and phosphate species (PO_4^{3-}), both of which are known to form readily when metal phosphides are exposed to air and supported by measurements taken in the Ni 2p region.[48] We speculate that the incomplete degradation of the MOF at 350 °C may partially explain why a nickel-rich $Ni_{12}P_5$ phase is visible in PXRD and TEM, caused by incomplete reaction of the Ni and P in the PCM precursor. This incomplete reaction means that not all of the catalyst is fully phosphorized at this temperature, which may impact its corresponding catalytic ability. On the other hand, the $Ni_{12}P_5$ formation at 550 °C is presumably due to the thermal decomposition of Ni_2P into $Ni_{12}P_5$ and phosphorus compounds/species, that is, the over-reduction of nickel species in Ni_2P.

3.2. Electrocatalytic Hydrogen Evolution Performance. In order to determine what effect the physical and chemical differences we observed above have on the various catalysts, we investigated the electrochemical activity of MOF-derived Ni_2P samples for the HER in a degassed 0.5 M H_2SO_4

DOI: 10.1021/acsaem.9b02109
ACS Appl. Energy Mater. 2020, 3, 176−183

electrolyte on GC substrates. Working electrodes with NiPCM-101-*T* samples (where *T* denotes the annealing temperature) at a mass loading of 0.5 mg/cm^2 were prepared by drop-casting a suspension of the sample being tested mixed in isopropyl alcohol on GC substrates. Linear scanning voltammetry (LSV) polarization (geometric current density vs potential) data for annealed NiPCM-101, benchmark platinum (Pt/C), and GC electrodes are shown in Figure 4a. The Pt/C electrode required the lowest overpotential (η_{10}) of 18 mV to achieve current densities of −10 mA/cm^2, and it exhibited the large background current because of its high surface area (Figure S10). For the nickel phosphides used in these experiments, our best-performing NiPCM-101-450 sample produced −10 mA/cm^2 of current density at 120 mV. Samples annealed at 350 and 550 °C were less active for the HER, both requiring 202 and 212 mV of overpotentials to produce −10 mA/cm^2 of current density, respectively. Here, the Tafel plots were determined for Pt/C and our nickel phosphide samples ($\eta = b \log|j| + a$; η, overpotential; b, Tafel slope; j, geometric current density). The resultant Tafel slopes were 14.7, 89.7, 60.9, and 65.0 mV/dec for Pt/C and NiPCM-101-350-550 electrodes, respectively (Figure 4b). The activity trend is reasonable considering the properties of films from our extensive characterization of samples. Diffractograms for samples annealed at 350 and 550 °C show significant contributions from a nickel-rich $Ni_{12}P_5$ phase which has been shown in separate studies of phase-controlled Ni−P catalysts to be less active for the HER than Ni_2P catalysts.[44,49,50] Pan et al. showed that while Ni_2P nanocrystals required 137 mV to produce −10 mA/cm^2 of current density, $Ni_{12}P_5$ samples required an additional 71 mV to reach similar current densities.[44] By controlling the annealing temperature used to prepare the catalyst from the PCM precursor, we can selectively produce the more active Ni_2P phase while limiting formation of the $Ni_{12}P_5$ phase, and therefore may improve the performance of the catalyst.

To further confirm the impact of the phase difference (Ni_2P vs $Ni_{12}P_5$) on the resultant HER activity, we compared the intrinsic activities of NiPCM-101-450 (only Ni_2P) and -550 (Ni_2P + $Ni_{12}P_5$) electrodes by checking the current densities based on electrochemically active surface areas (ECSAs), which were determined by electrochemical C_{dl}'s (see Figure S1 and Figure 4c), at a certain applied potential (E_{appl} = −150 mV vs RHE). As shown in Figure 4c, NiPCM-101-450 showed a higher roughness factor [RF = C_{dl}/(geometric electrode-area: 0.19625 cm^2)] of 379.1 than NiPCM-101-550 (RF = 219.7) which might be because NiPCM-101-550 could form large agglomerations due to the high annealing temperature, resulting in a lower ECSA. At −150 mV vs RHE (Figure 4d), NiPCM-101-450 exhibited a quite high HER activity based on ECSA (∼−71 μA/cm$^2_{ECSA}$), which was about 13 times greater than that of NiPCM-101−550 (∼−5.5 μA/cm$^2_{ECSA}$). Accordingly, the presence of $Ni_{12}P_5$ results in a low HER intrinsic activity and a negative impact on the overall HER geometric performance.

The electrode stability was also evaluated by electrochemical and analytical degradation tests in 0.5 M H_2SO_4. First, an amperometric experiment was conducted over a 1 h period with a rotating disk electrode system (rotation speed: 1600 rpm), which was used to remove the evolved hydrogen bubbles from the electrode surface, in order to investigate the electrochemical and physical stability of the best PCM-derived Ni_2P catalyst (NiPCM-101-450) with Nafion support for the HER. Here, the introduced Nafion support may be able to minimize the physical detachment of our catalyst powder from the substrate. The results presented in Figure S11 show that the current produced at −0.138 V vs RHE suggests a slight degradation of the electrode during the duration of the test. To examine the reason for this electrode degradation, the electrochemical stability of our catalyst was further confirmed by conducting a Faradaic efficiency test without rotating the electrode. It was reported that Nafion can suppress the corrosion of Ni_2P in 0.5 M H_2SO_4.[13] In order to evaluate a true electrochemical stability of our Ni_2P catalyst, the Nafion support was intentionally not used for the Faradaic efficiency test. As seen in Figure S12, the Faradaic efficiency of 91 ± 5% was recorded for a 1 h HER test, which implies that a small portion of the applied electrons might be used for a side reaction corresponding to chemical degradation of our Ni_2P catalyst. Previously, Schaak et al. also confirmed the significant chemical degradation of Ni_2P nanoparticles in 0.5 M H_2SO_4.[13] From the above discussion, we concluded that the electrode degradation was probably due to some chemical degradation and physical detachment of the Ni_2P. A study to enhance the chemical and physical stability of Ni_2P is ongoing.

While our PCM-derived synthesis allows us to selectively target the active Ni_2P phase and show relatively high HER performance, it is also important to note that the overpotential of our best-performing MOF-derived sample (NiPCM-101-450: η_{10} = 120 mV and η_{20} = 140 mV) compares favorably with other reported Ni_2P-based catalysts on GC substrates (Table S1). In particular, our sample compares well with other MOF-derived samples prepared with secondary phosphorus sources. For instance, Ni_2P polyhedra made by annealing MOF-74 together with sodium hypophosphite required overpotentials of 158 mV at −10 mA/cm^2.[51] Surprisingly, Ni_2P nanoparticles (1 mg/cm^2) on Ti foil reported by Schaak et al. required a lower overpotential of 130 mV to achieve −20 mA/cm^2 compared with other nanoparticle-loaded plain substrate (i.e., GC) electrodes, which might be because of the high conductivity of the Ti foil.[13] Additionally, high-surface-area substrates such as a nickel foam can also boost the HER geometric activity. Therefore, by using highly conductive substrates with high surface areas, our sample may be able to show further enhanced HER performance. From these comparisons to literature values, it is immediately apparent not only that we can select for the more active nickel phosphide phase (Ni_2P), but also that the resulting catalyst shows a similar/better HER activity than catalysts produced by other means. This may be the result of the increased surface area of the catalyst or the presence of the carbon shell (Figure 2): the carbon shell can presumably (i) optimize the Gibbs free energy of hydrogen adsorption on the catalyst surface, (ii) enhance electrical conductivity, and also (iii) improve durability.[52,53] Further work will be necessary to determine if there is a single factor that explains the performance. Nonetheless, this study establishes the synthesis of metal phosphide from tailored organophosphine-based MOFs as a preferential route toward making active HER catalysts.

4. CONCLUSIONS

In summary, we have used a phosphine-based MOF, NiPCM-101, as a solid single-source precursor for the synthesis of nickel phosphide hydrogen evolution catalysts. Past reports in the literature taking advantage of the high surface area of MOFs in the synthesis of catalysts required separate precursors

DOI: 10.1021/acsaem.9b02109
ACS Appl. Energy Mater. 2020, 3, 176−183

for the metal and phosphorus. In our work, however, the phosphorus content of the metal phosphide is provided by the triphenylphosphine organic ligands inherently incorporated into the structure of the PCMs. The use of such an air-stable solid-state precursor is convenient and offers better control of the synthesis of metal phosphides compared with other MOFs that require an exogenous P source. We used the Ni_2P samples derived from this MOF as a hydrogen evolution catalyst and achieved current densities of −10 mA/cm^2 at an overpotential of 120 mV.

■ ASSOCIATED CONTENT

Supporting Information

The Supporting Information is available free of charge at https://pubs.acs.org/doi/10.1021/acsaem.9b02109.

Experimental and characterization details as well as further analysis (PDF)

■ AUTHOR INFORMATION

Corresponding Authors

*E-mail: smh@cm.utexas.edu.
*E-mail: mullins@che.utexas.edu.

ORCID

Kenta Kawashima: 0000-0001-7318-6115
Simon M. Humphrey: 0000-0001-5379-4623
C. Buddie Mullins: 0000-0003-1030-4801

Notes

The authors declare no competing financial interest.

■ ACKNOWLEDGMENTS

The authors gratefully acknowledge the National Science Foundation for Grants CHE-1664941 (C.B.M.) and DMR-1506694 (S.M.H.) and the Welch Foundation for Grants F-1436 (C.B.M.) and F-1738 (S.M.H.). O.M. gratefully acknowledges a National Science Foundation (NSF) Integrative Graduate Education and Research Traineeship (IGERT) Grant 0966298 for financial support. We also acknowledge the National Science Foundation (Grant 0618242) for funding the X-ray photoelectron spectrometer used in this work.

■ REFERENCES

(1) Lewis, N. S.; Nocera, D. G. Powering the Planet: Chemical Challenges in Solar Energy Utilization. *Proc. Natl. Acad. Sci. U. S. A.* **2006**, *103* (43), 15729−15735.

(2) Grätzel, M.; Gr, M. Photoelectrochemical Cells. *Nature* **2001**, *414* (6861), 338−344.

(3) Bard, A. J.; Fox, M. A. Artificial Photosynthesis: Solar Splitting of Water to Hydrogen and Oxygen Water Splitting. *Acc. Chem. Res.* **1995**, *28* (28), 141−145.

(4) Turner, J. A. Sustainable Hydrogen Production. *Science (Washington, DC, U. S.)* **2004**, *305* (5686), 972−974.

(5) Nocera, D. G. Personalized Energy: The Home as a Solar Power Station and Solar Gas Station. *ChemSusChem* **2009**, *2* (5), 387−390.

(6) Norskov, J. K.; Christensen, C. H. Toward Efficient Hydrogen Production at Surfaces. *Science (Washington, DC, U. S.)* **2006**, *312* (5778), 1322−1323.

(7) Nørskov, J. K.; Bligaard, T.; Logadottir, A.; Kitchin, J. R.; Chen, J. G.; Pandelov, S.; Stimming, U. Trends in the Exchange Current for Hydrogen Evolution. *J. Electrochem. Soc.* **2005**, *152* (3), J23−J26.

(8) Greeley, J.; Nørskov, J. K.; Kibler, L. A.; El-Aziz, A. M.; Kolb, D. M. Hydrogen Evolution Over Bimetallic Systems: Understanding the Trends. *ChemPhysChem* **2006**, *7* (5), 1032−1035.

(9) McKone, J. R.; Marinescu, S. C.; Brunschwig, B. S.; Winkler, J. R.; Gray, H. B. Earth-Abundant Hydrogen Evolution Electrocatalysts. *Chem. Sci.* **2014**, *5* (3), 865−878.

(10) Chen, W.-F.; Muckerman, J. T.; Fujita, E. Recent Developments in Transition Metal Carbides and Nitrides as Hydrogen Evolution Electrocatalysts. *Chem. Commun. (Cambridge, U. K.)* **2013**, *49* (79), 8896−8909.

(11) Hinnemann, B.; Moses, P. G.; Bonde, J.; Jørgensen, K. P.; Nielsen, J. H.; Horch, S.; Chorkendorff, I.; Nørskov, J. K. Biomimetic Hydrogen Evolution: MoS_2 Nanoparticles as Catalyst for Hydrogen Evolution. *J. Am. Chem. Soc.* **2005**, *127* (15), 5308−5309.

(12) Vesborg, P. C. K.; Seger, B.; Chorkendorff, I. Recent Development in Hydrogen Evolution Reaction Catalysts and Their Practical Implementation. *J. Phys. Chem. Lett.* **2015**, *6* (6), 951−957.

(13) Popczun, E. J.; McKone, J. R.; Read, C. G.; Biacchi, A. J.; Wiltrout, A. M.; Lewis, N. S.; Schaak, R. E. Nanostructured Nickel Phosphide as an Electrocatalyst for the Hydrogen Evolution Reaction. *J. Am. Chem. Soc.* **2013**, *135* (25), 9267−9270.

(14) Feng, L.; Vrubel, H.; Bensimon, M.; Hu, X. Easily-Prepared Dinickel Phosphide (Ni_2P) Nanoparticles as an Efficient and Robust Electrocatalyst for Hydrogen Evolution. *Phys. Chem. Chem. Phys.* **2014**, *16* (13), 5917−5921.

(15) Tian, J.; Liu, Q.; Asiri, A. M.; Sun, X. Self-Supported Nanoporous Cobalt Phosphide Nanowire Arrays: An Efficient 3D Hydrogen-Evolving Cathode over the Wide Range of PH 0−14. *J. Am. Chem. Soc.* **2014**, *136* (21), 7587−7590.

(16) Popczun, E. J.; Read, C. G.; Roske, C. W.; Lewis, N. S.; Schaak, R. E. Highly Active Electrocatalysis of the Hydrogen Evolution Reaction by Cobalt Phosphide Nanoparticles. *Angew. Chem.* **2014**, *126* (21), 5531−5534.

(17) Shi, Y.; Zhang, B. Recent Advances in Transition Metal Phosphide Nanomaterials: Synthesis and Applications in Hydrogen Evolution Reaction. *Chem. Soc. Rev.* **2016**, *45* (6), 1529−1541.

(18) Jiang, P.; Liu, Q.; Liang, Y.; Tian, J.; Asiri, A. M.; Sun, X. A Cost-Effective 3D Hydrogen Evolution Cathode with High Catalytic Activity: FeP Nanowire Array as the Active Phase. *Angew. Chem., Int. Ed.* **2014**, *53* (47), 12855−12859.

(19) Callejas, J. F.; McEnaney, J. M.; Read, C. G.; Crompton, J. C.; Biacchi, A. J.; Popczun, E. J.; Gordon, T. R.; Lewis, N. S.; Schaak, R. E. Electrocatalytic and Photocatalytic Hydrogen Production from Acidic and Neutral-PH Aqueous Solutions Using Iron Phosphide Nanoparticles. *ACS Nano* **2014**, *8* (11), 11101−11107.

(20) Jiang, N.; You, B.; Sheng, M.; Sun, Y. Electrodeposited Cobalt-Phosphorous-Derived Films as Competent Bifunctional Catalysts for Overall Water Splitting. *Angew. Chem., Int. Ed.* **2015**, *54* (21), 6251−6254.

(21) McEnaney, J. M.; Crompton, J. C.; Callejas, J. F.; Popczun, E. J.; Read, C. G.; Lewis, N. S.; Schaak, R. E. Electrocatalytic Hydrogen Evolution Using Amorphous Tungsten Phosphide Nanoparticles. *Chem. Commun.* **2014**, *50* (75), 11026−11028.

(22) Xing, Z.; Liu, Q.; Asiri, A. M.; Sun, X. High-Efficiency Electrochemical Hydrogen Evolution Catalyzed by Tungsten Phosphide Submicroparticles. *ACS Catal.* **2015**, *5* (1), 145−149.

(23) Xiao, P.; Sk, M. A.; Thia, L.; Ge, X.; Lim, R. J.; Wang, J.-Y.; Lim, K. H.; Wang, X. Molybdenum Phosphide as an Efficient Electrocatalyst for the Hydrogen Evolution Reaction. *Energy Environ. Sci.* **2014**, *7* (8), 2624−2629.

(24) Huang, Z.; Chen, Z.; Chen, Z.; Lv, C.; Humphrey, M. G.; Zhang, C. Cobalt Phosphide Nanorods as an Efficient Electrocatalyst for the Hydrogen Evolution Reaction. *Nano Energy* **2014**, *9*, 373−382.

(25) Jiang, P.; Liu, Q.; Ge, C.; Cui, W.; Pu, Z.; Asiri, A. M.; Sun, X. CoP Nanostructures with Different Morphologies: Synthesis, Characterization and a Study of Their Electrocatalytic Performance toward the Hydrogen Evolution Reaction. *J. Mater. Chem. A* **2014**, *2* (35), 14634−14640.

(26) Stern, L.-A.; Feng, L.; Song, F.; Hu, X. Ni_2P as a Janus Catalyst for Water Splitting: The Oxygen Evolution Activity of Ni_2P Nanoparticles. *Energy Environ. Sci.* **2015**, *8* (8), 2347.

DOI: 10.1021/acsaem.9b02109
ACS Appl. Energy Mater. 2020, 3, 176−183

(27) Oyama, S. T. Novel Catalysts for Advanced Hydroprocessing: Transition Metal Phosphides. *J. Catal.* **2003**, *216* (1−2), 343−352.
(28) Liu, P.; Rodriguez, J. A. Catalysts for Hydrogen Evolution from the [NiFe] Hydrogenase to the Ni_2P (001) Surface: The Importance of Ensemble Effect. *J. Am. Chem. Soc.* **2005**, *127* (42), 14871−14878.
(29) Liu, Q.; Tian, J.; Cui, W.; Jiang, P.; Cheng, N.; Asiri, A. M.; Sun, X. Carbon Nanotubes Decorated with CoP Nanocrystals: A Highly Active Non-noble-metal Nanohybrid Electrocatalyst for Hydrogen Evolution. *Angew. Chem., Int. Ed.* **2014**, *53* (26), 6710−6714.
(30) Wang, D.-Y.; Gong, M.; Chou, H.-L.; Pan, C.-J.; Chen, H.-A.; Wu, Y.; Lin, M.-C.; Guan, M.; Yang, J.; Chen, C.-W.; et al. Highly Active and Stable Hybrid Catalyst of Cobalt-Doped FeS_2 Nanosheets−carbon Nanotubes for Hydrogen Evolution Reaction. *J. Am. Chem. Soc.* **2015**, *137* (4), 1587−1592.
(31) Yu, X.-Y.; Feng, Y.; Guan, B.; Lou, X. W. D.; Paik, U. Carbon Coated Porous Nickel Phosphides Nanoplates for Highly Efficient Oxygen Evolution Reaction. *Energy Environ. Sci.* **2016**, *9* (4), 1246−1250.
(32) Wu, H. B.; Lou, X. W. D. Metal-Organic Frameworks and Their Derived Materials for Electrochemical Energy Storage and Conversion: Promises and Challenges. *Sci. Adv.* **2017**, *3* (12), No. eaap9252.
(33) Zhang, H.; Nai, J.; Yu, L.; Lou, X. W. D. Metal-Organic-Framework-Based Materials as Platforms for Renewable Energy and Environmental Applications. *Joule* **2017**, *1* (1), 77−107.
(34) Hu, E.; Feng, Y.; Nai, J.; Zhao, D.; Hu, Y.; Lou, X. W. D. Construction of Hierarchical Ni−Co−P Hollow Nanobricks with Oriented Nanosheets for Efficient Overall Water Splitting. *Energy Environ. Sci.* **2018**, *11* (4), 872−880.
(35) Lu, X. F.; Yu, L.; Lou, X. W. D. Highly Crystalline Ni-Doped FeP/Carbon Hollow Nanorods as All-PH Efficient and Durable Hydrogen Evolving Electrocatalysts. *Sci. Adv.* **2019**, *5* (2), No. eaav6009.
(36) Nuñez, A. J.; Chang, M. S.; Ibarra, I. A.; Humphrey, S. M. Tuning the Host−Guest Interactions in a Phosphine Coordination Polymer through Different Types of Post-Synthetic Modification. *Inorg. Chem.* **2014**, *53* (1), 282−288.
(37) Dunning, S. G.; Nandra, G.; Conn, A. D.; Chai, W.; Sikma, R. E.; Lee, J. S.; Kunal, P.; Reynolds, J. E., III; Chang, J.; Steiner, A.; et al. A Metal−Organic Framework with Cooperative Phosphines That Permit Post-Synthetic Installation of Open Metal Sites. *Angew. Chem.* **2018**, *130* (30), 9439−9443.
(38) Bohnsack, A. M.; Ibarra, I. A.; Hatfield, P. W.; Yoon, J. W.; Hwang, Y. K.; Chang, J.-S.; Humphrey, S. M. High Capacity CO_2 Adsorption in a Mg (Ii)-Based Phosphine Oxide Coordination Material. *Chem. Commun.* **2011**, *47* (17), 4899−4901.
(39) Ibarra, I. A.; Hesterberg, T. W.; Holliday, B. J.; Lynch, V. M.; Humphrey, S. M. Gas Sorption and Luminescence Properties of a Terbium (Iii)-Phosphine Oxide Coordination Material with Two-Dimensional Pore Topology. *Dalt. Trans.* **2012**, *41* (26), 8003−8009.
(40) Ibarra, I. A.; Yoon, J. W.; Chang, J.-S.; Lee, S. K.; Lynch, V. M.; Humphrey, S. M. Organic Vapor Sorption in a High Surface Area Dysprosium (III)−Phosphine Oxide Coordination Material. *Inorg. Chem.* **2012**, *51* (22), 12242−12247.
(41) Humphrey, S. M.; Allan, P. K.; Oungoulian, S. E.; Ironside, M. S.; Wise, E. R. Metal−organophosphine and Metal−organophosphonium Frameworks with Layered Honeycomb-like Structures. *Dalt. Trans.* **2009**, *13*, 2298−2305.
(42) Ibarra, I. A.; Tan, K. E.; Lynch, V. M.; Humphrey, S. M. CO_2 Adsorption Properties of a Ca (Ii)-Based Organophosphonium Coordination Material. *Dalt. Trans.* **2012**, *41* (14), 3920−3923.
(43) Sun, M.; Liu, H.; Qu, J.; Li, J. Earth-Rich Transition Metal Phosphide for Energy Conversion and Storage. *Adv. Energy Mater.* **2016**, *6* (13), 1600087.
(44) Pan, Y.; Liu, Y.; Zhao, J.; Yang, K.; Liang, J.; Liu, D.; Hu, W.; Liu, D.; Liu, Y.; Liu, C. Monodispersed Nickel Phosphide Nanocrystals with Different Phases: Synthesis, Characterization and Electrocatalytic Properties for Hydrogen Evolution. *J. Mater. Chem. A* **2015**, *3* (4), 1656−1665.
(45) Lu, Y.; Tu, J.; Xiong, Q.; Zhang, H.; Gu, C.; Wang, X.; Mao, S. X. Large-Scale Synthesis of Porous Ni_2P Nanosheets for Lithium Secondary Batteries. *CrystEngComm* **2012**, *14* (24), 8633−8641.
(46) Ge, Y.; Dong, P.; Craig, S. R.; Ajayan, P. M.; Ye, M.; Shen, J. Transforming Nickel Hydroxide into 3D Prussian Blue Analogue Array to Obtain Ni_2P/Fe_2P for Efficient Hydrogen Evolution Reaction. *Adv. Energy Mater.* **2018**, *8* (21), 1800484.
(47) Watts, J. F.; Wolstenholme, J. *An Introduction to Surface Analysis by XPS and AES*; Wiley-VCH, 2003; pp 224.
(48) Xing, Z.; Liu, Q.; Asiri, A. M.; Sun, X. Closely Interconnected Network of Molybdenum Phosphide Nanoparticles: A Highly Efficient Electrocatalyst for Generating Hydrogen from Water. *Adv. Mater.* **2014**, *26* (32), 5702−5707.
(49) Kucernak, A. R. J.; Naranammalpuram Sundaram, V. N. Nickel Phosphide: The Effect of Phosphorus Content on Hydrogen Evolution Activity and Corrosion Resistance in Acidic Medium. *J. Mater. Chem. A* **2014**, *2* (41), 17435−17445.
(50) Li, H.; Lu, S.; Sun, J.; Pei, J.; Liu, D.; Xue, Y.; Mao, J.; Zhu, W.; Zhuang, Z. Phase-Controlled Synthesis of Nickel Phosphide Nanocrystals and Their Electrocatalytic Performance for the Hydrogen Evolution Reaction. *Chem. - Eur. J.* **2018**, *24* (45), 11748−11754.
(51) Yan, L.; Dai, P.; Wang, Y.; Gu, X.; Li, L.; Cao, L.; Zhao, X. In Situ Synthesis Strategy for Hierarchically Porous Ni_2P Polyhedrons from MOFs Templates with Enhanced Electrochemical Properties for Hydrogen Evolution. *ACS Appl. Mater. Interfaces* **2017**, *9* (13), 11642−11650.
(52) Lu, J.; Yin, S.; Shen, P. K. Carbon-Encapsulated Electrocatalysts for the Hydrogen Evolution Reaction. *Electrochem. Energy Rev.* **2019**, *2* (1), 105−127.
(53) Chung, D. Y.; Jun, S. W.; Yoon, G.; Kim, H.; Yoo, J. M.; Lee, K. S.; Kim, T.; Shin, H.; Sinha, A. K.; Kwon, S. G.; Kang, K.; Hyeon, T.; Sung, Y. E. Large-Scale Synthesis of Carbon-Shell-Coated FeP Nanoparticles for Robust Hydrogen Evolution Reaction Electrocatalyst. *J. Am. Chem. Soc.* **2017**, *139* (19), 6669−6674.

■ NOTE ADDED AFTER ASAP PUBLICATION

This paper was published ASAP on December 13, 2019, with a few minor text errors. The corrected version was reposted on December 18, 2019.

DOI: 10.1021/acsaem.9b02109
ACS Appl. Energy Mater. 2020, 3, 176−183